# Hybrid sensorless control of axial flux permanent magnet motor drives, including zero speed

# Hybrid sensorless control of Axial Flux Permanent Magnet motor drives, including zero speed

Paolo Giangrande[*], Davide Ronchetto[†], Gianmario Pellegrino[†],
Francesco Cupertino[*], Christopher Gerada‡ and Mark Sumner‡

[*]Politecnico di Bari
Italy

[†]Politecnico di Torino
Italy

‡University of Nottingham
United Kingdom

E-Mail: giangrande@deemail.poliba.it

## Keywords

«Control of drive», «Drive», «Sensorless control», «Traction application», «Permanent magnet motor».

## Abstract

The sensorless control of an axial flux permanent magnet motor drive is proposed and tested. The motor is not purposely designed for sensorless control and shows a very small inherent saliency. This significantly affects the saliency-based position estimation in the low speed region. Other non-idealities, such as the non-sinusoidal back-EMF waveforms and possible misalignment between stator and rotor are also evidenced. A robust sensorless control scheme is proposed, able to deal with these non-idealities and with a rather simple implementation. The position estimation is based on a closed loop hybrid observer of the permanent magnet flux linkage. Experimental results report torque and speed sensorless control.

## Introduction

Axial flux permanent magnet machines are disk-shaped machines characterized by their compactness and high torque density [1]. The short axial length can facilitate the mechanical integration into compact drivelines, while the specific shape makes them suited for high pole numbers. For these reasons they are well suited for direct drive applications and have been particularly proposed for electric and hybrid vehicle drivetrains [2] and wind generators [3]. Mounting motion sensors in a highly integrated environment can pose significant challenges.

Sensorless control can be an adopted primary solution or an emergency backup, to improve the reliability of the drive. Other benefits include cost reduction and improved reliability due to the often challenging environmental conditions. As for a radial flux synchronous PM machine, the motor position can be estimated at standstill and low speed by tracking the saliency by means of signal injection [4-5] and at higher speeds by model-based methods, such as those relying on back-electromotive force (EMF) integration [6]. Hybrid methods mix the two types of estimation over the speed range of the drive [7]. Most of the referenced works refer to radial flux motors, with few exceptions [8]. Despite the commonalities, axial flux machines can be more challenging to control than radial flux machines due to several inherent phenomena. These include the variable saturation level along the machine radius (i.e. from the inner to the outer diameter of the machine), the significant 3-D effects and the airgap length generally has a significant variation due to the complex mechanical structure and significant axial forces.

A robust hybrid, sensorless control scheme for a double-sided axial flux PM machine is proposed within this work, capable of controlling the machine from zero to maximum speed. The position tracking is based on rotating voltage injection at standstill and very low speed and on back-EMF integration at higher speed. As already mentioned, the control is tested on a machine with very little saliency ($L_d$ = 1.055 mH, $L_q$ = 1.0 mH) and with significant non-idealities. At higher speed, a model based scheme is used for the position estimation. The back-emf of the tested motor are non sinusoidal,

and this produces a position estimation error and in particular a significant ripple on the estimated speed.
The control robustness is thoroughly tested and implementation details is provided. A first test shows the performance of the sensorless hybrid observer in torque control mode from standstill to 30% of the base speed, at no load and at load. A second experiment shows the operation in closed loop sensorless speed control. The effects of rotor misalignment and magnetic field harmonics in the presented waveforms are evidenced.

## Axial flux machine

The motor under test is a double sided machine, with toroidal stator windings. The machine is totally enclosed and water cooled and has been designed for hybrid traction. Its ratings are presented in the "Experimental results" section. The two rotors are offset by half a stator slot pitch for mitigating the cogging torque, as represented in the schematic layout of the machine reported in Fig. 1.

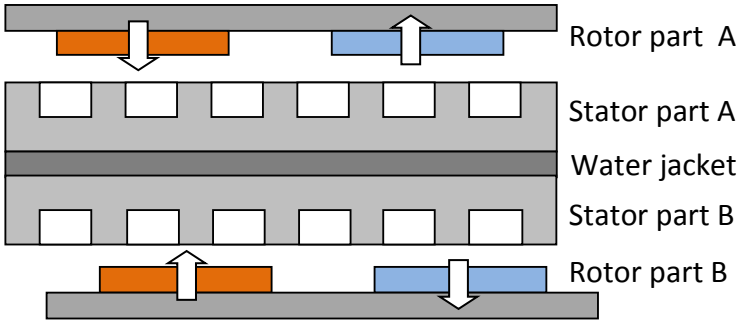


Fig. 1: Schematic representation of the double sided, axial flux, surface mounted PM synchronous machine under test. The two rotor sides are offset by half slot pitch.

The fundamental saliency is very low despite having soft magnetic pole-pieces on the d-axis to increase the machine inductance as discussed in [9-10]. Fig.2 shows the basic rotor structure in which the soft composite pieces have been introduced in the inner ring of the two rotor plates. The soft magnetic composite is Somaloy 700 [11].

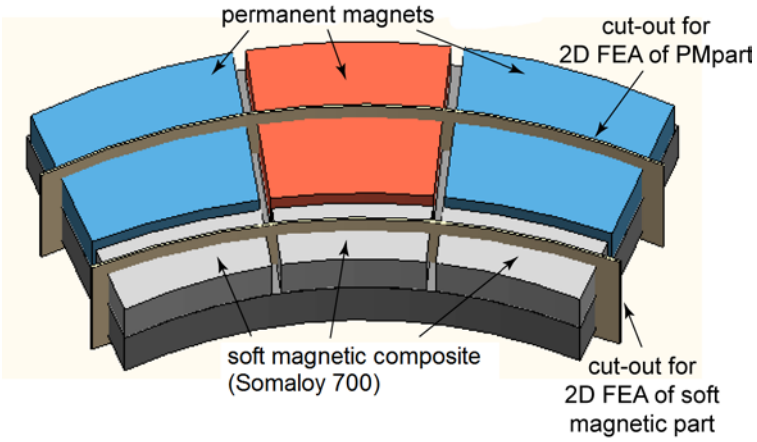


Fig. 2: Sketch of the two part rotor double-sided axial flux PM machine.

## Hybrid rotor position observer

### Low speed, saliency-based estimation

The rotor position estimation at low speed is based on the injection of a rotating voltage signal in the stationary frame [4-5].

The injected voltage, high frequency component is:

$$\bar{v}_{s,HF} = V_{inj} \cdot e^{j\omega_{inj}t} \tag{1}$$

where the vector amplitude is $V_{inj}$ = 45 V and the angular frequency is $\omega_{inj} = 500 \cdot 2\pi$ rad/s.
Under the assumption of a sinusoidal fundamental saliency, the resulting current vector consists of a positive and a negative-sequence component:

$$\bar{i}_{s,HF} = I_p \cdot e^{j\left(\omega_{inj}t - 90°\right)} + I_n \cdot e^{j\left(2\theta - \omega_{inj}t + 90°\right)} \tag{2}$$

where θ is the rotor electrical position. The amplitude of the negative sequence component depends on the motor saliency, according to:

$$I_n = \frac{V_{inj}}{\omega_{inj}} \cdot \frac{\Delta L_s}{L_s^2 - \Delta L_s^2} \tag{3}$$

where

$$L_s = \tfrac{1}{2} \cdot \left(L_d + L_q\right), \; \Delta L_s = \tfrac{1}{2} \cdot \left(L_d - L_q\right) \tag{4}$$

The negative-sequence current is used for tracking the rotor position electrical angle θ by means of the standard scheme reported in Fig. 3, where the position observer scheme is simply a proportional-integral regulator. The considered prototype revealed an extreme sensitivity of its saliency to the actual position of the fundamental current vector. The positioning of the pole pieces as in Fig. 2 (along the *d*-axis) produces a small positive saliency ($L_d > L_q$) that is counteracted by the negative saliency ($L_d < L_q$) of the PM section of the machine. The result is a very low saliency figure ($L_s$ = 1.027 mH and $\Delta L_s$ = 0.027 mH) that is also quite sensitive to the load conditions ($i_q$) and, in particular, very sensitive to eventual $i_d$ components, as came out from various tests using different current phase angles.
Such sensitivity made the pulsating injection based sensorless schemes unfeasible for this motor, since any transient estimation error produces an unwilled *d*-axis fundamental current component that perturbs the saliency and leads the position estimation to instability.

## Model-based estimation

Above the very low speed range, the motor flux linkage can be accurately estimated by back-EMF integration, and from the flux the rotor position. The rotor flux is obtained as in (5) by subtraction of the current dependent flux linkage component.

$$\bar{\lambda}_m = \int \left(\bar{v}_s - R_s \cdot \bar{i}_s\right) \cdot dt - L_s \cdot \bar{i}_s \tag{5}$$

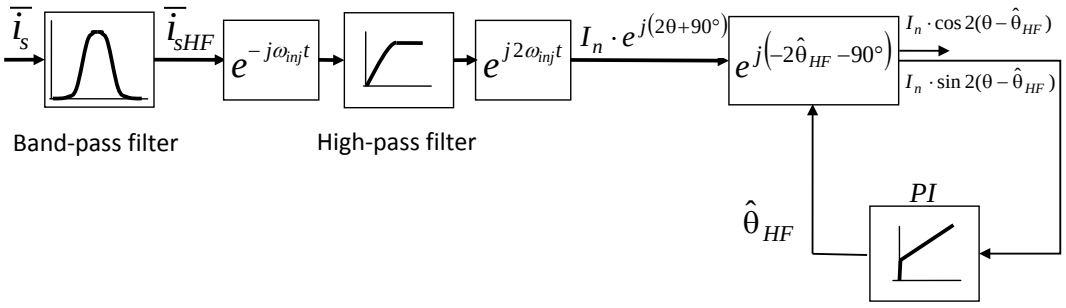


Fig. 3: Injection based estimation of the rotor position: current demodulation speed and position tracking loop.

The average value $L_s$ (4) has been used instead of the *dq* inductances $L_d$ and $L_q$ for simplicity due to the low saliency of this particular machine. A more complex scheme, in synchronous coordinates, would be otherwise required for motors with a significant saliency ($L_d \neq L_q$) [10]. Under the hypothesis of sinusoidal flux linkage, the position of the estimated rotor flux would coincide with the electrical position of the rotor:

$$\bar{\lambda}_m = \lambda_m \cdot (\cos\theta + j \sin\theta) \tag{6}$$

However, this is not the case here, as pointed out by the trapezoidal phase back-EMF waveform represented in Fig.4, and the position estimation sine and cosine components are distorted with respect to equation (6).

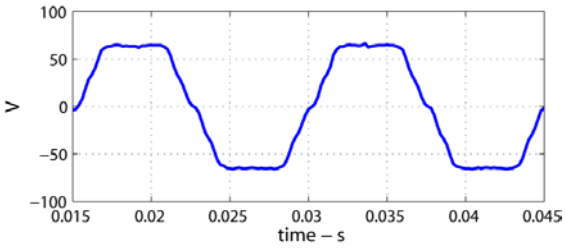


Fig. 4: Phase back-EMF measured at 500 rpm.

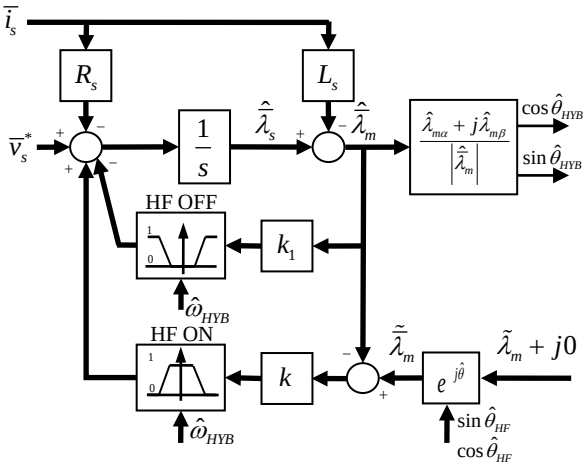


Fig.5 Hybrid flux observer scheme.

## Hybrid flux observer

The flux observer scheme, reported in Fig. 5, is similar to the ones proposed in [6-7]. The command voltages are used instead of the measured ones. A negative feed-back is needed to avoid the model-based flux integrator to drift due to offsets.

Different feedback signals are used at low and high speed, according to the speed dependent blocks "HF ON" and "HF OFF". At low speed (< 100 rpm, i.e. 13 Hz) the feedback is referenced by a flux estimate based on the HF injection position estimation. The gain *k* (30 rad/s) determines the crossover frequency between the injection-based estimate and the model-based estimate. At speeds higher than 120 rpm (i.e. 16 Hz) the HF signal injection is turned off and the feedback signal is substituted with a low gain feedback of the model-based estimate itself. The gain $k_1$ (10 rad/s) has been chosen as low as possible to avoid amplitude attenuation and phase delay in the flux estimate [6]. Between the two speed thresholds (100 ÷ 120 rpm) the two feed-backs are mixed proportionally to the estimated speed by the two switching blocks. As the speed increases, the amplitude of the HF injected voltage is progressively reduced by the same "HF ON" function used for the feed-back. For the sake of simplicity, the speed estimate signal that commands the HF ON and OFF blocks is obtained by cross-product of the stator flux and back-EMF signal components [12], according to:

$$\omega_{HYB} = \frac{\lambda_{s\alpha} e_{s\beta} - \lambda_{s\beta} e_{s\alpha}}{\left|\lambda_s^2\right|} \tag{7}$$

The back-EMF signals $e_{s\alpha}$, $e_{s\beta}$ in (7) are the input of the integrator of Fig. 5. Due to back-EMF harmonics and distortion due to rotor misalignment, the speed signal (7) needs filtering to avoid the false triggering or the noisy triggering of the HF ON/OFF blocks of Fig. 5.

When closed loop sensorless speed control is needed, the simple estimation in (7) is too noisy to be a proper speed feedback and a more refined speed observer structure must be adopted, as reported in Fig. 6.

# Experimental results

## Control scheme

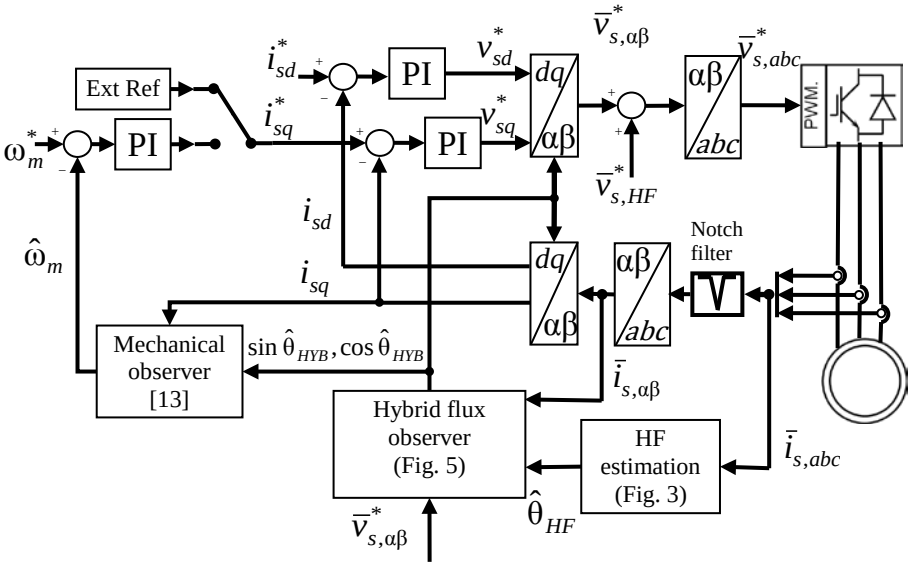


Fig. 6: The sensorless speed and torque control.

The sensorless control scheme is reported in Fig. 6: torque control and closed loop speed control operation are investigated in the following.

In particular, the high-frequency injected voltage ($\bar{v}^*_{s,HF}$) is activated and deactivated by the same HF ON block reported in Fig. 5 and not reproduced in Fig. 6 for space reasons.

The "HF estimation" block is the one reported in Fig. 3 and estimates the rotor position at low speed. The "hybrid flux observer" block is the one of Fig.5 and merges the saliency based position estimation with the back-emf based estimation. Such block includes the noisy speed estimation (7), for the sake of commanding the HF ON and HF OFF blocks of Fig. 5. Such speed estimate is very distorted, as shown in Fig. 7 and is heavily filtered for the switching blocks purpose (e.g. 1 Hz cut-off low pass filter) to avoid false trips.

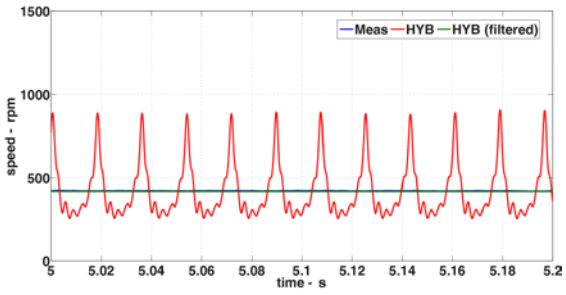


Fig. 7: Speed measured and calculated with the hybrid observer (filtered at 1 Hz and not filtered) at 420 rpm, steady state.

For closed loop speed control the mechanical observer block [13] is included, providing a smooth speed feedback with a more adequate dynamic response.

## Description of the experimental setup

The experimental rig depicted in Fig. 8 consists of the axial flux machine under test coupled with a DC motor. The two machines are connected by means of a flexible coupling.
The axial-flux machine ratings are 200 Nm continuous torque at 1400 rpm (30 kW), 300 Nm intermittent overload, 100 A (pk) continuous current, 400 V (pk) phase to phase rated voltage. The torque factor of the machine is then 2 Nm/A (pk). The pole pairs are eight. The motor is fed by an industrial three-phase inverter rated 91 A (pk) and 590 V bus voltage, provided of a custom interface board to receive the PWM commands either from its embedded controlled or from an outer independent controller. The controller, in this case, is a dSPACE 1104 microcontroller board whose PWM signals are transmitted to the inverter through fiber optic. The axial-flux machine is oversized if compared to the three phase inverter. For this reason the inverter will be substituted with one of bigger size in the future.
The DC motor has a continuous torque of 500 Nm at 850 rpm (44 kW), 430 V and 113 A. It can be either speed controlled or torque controlled by means of an industrial three-phase full bridge dual converter (4 quadrants) whose ratings are 600 V and 360 A.

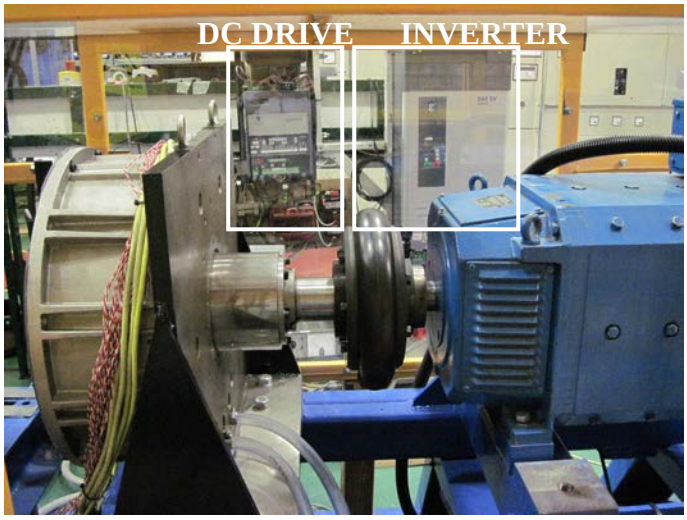


Fig.8: The experimental rig: the motor to the left is the axial-flux PM machine which is connected to the DC motor (right side). Behind them the DC drive (left) and the three phase inverter (right) are evidenced.

## Torque sensorless control

At first, the DC motor is speed controlled and the axial-flux machine is torque controlled. The start-up sequence represented in Fig. 9 demonstrates the robustness of the control at low and medium speed, at no load and at 60 Nm load. After the control commissioning sequence, the high frequency injection is enabled. Once the position is detected, current control is enabled at zero speed, at first with zero current reference. At time 0 s a ramp torque reference of 60 Nm (30 A) is set. The speed varies slightly due to the poor performance of the DC motor drive speed controller. However, the sensorless control is stable at very low speed (1 Hz or 7.5 rpm) with load.
The speed is then ramped up by the DC motor drive to 400 rpm. The ramp is slow to emphasize the smooth transition between the low speed and high speed observer schemes, which occurs around time 2.7 s (between 100 and 120 rpm as highlighted in Fig. 10).
The torque current ($i_q$) is distorted by the back-EMF harmonics (as already discussed), this being proportional with speed. The reported estimated speed (indicated as HYB, filtered in the figure) is the signal used to command the two switching blocks HF ON and HF OFF in Fig. 5. As said, this is estimated according to (7) and then filtered with 1 Hz cut-off frequency (-3dB). The effect of filtering is put in evidence by the significant delay of the estimated signal with respect to the measured speed, controlled by the DC motor drive.

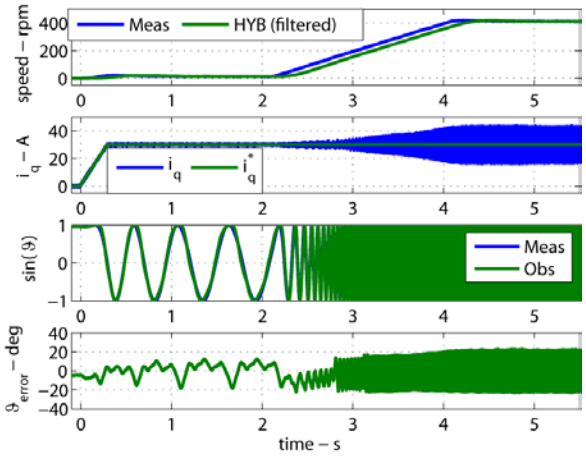


Fig. 9: Sensorless torque control: start-up sequence from zero speed, no load, to 400 rpm, 30 A load (60 Nm).

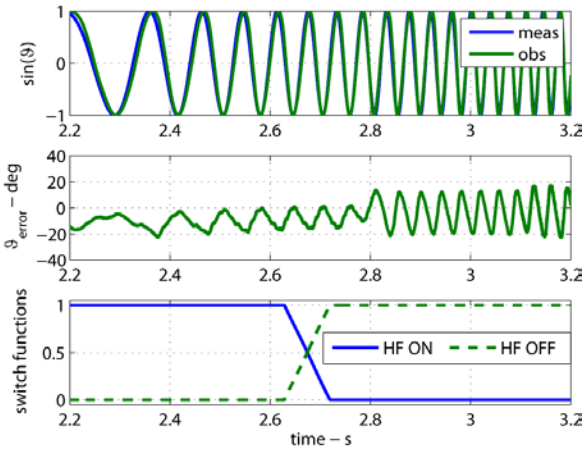


Fig. 10: Transition between low speed and high speed modes of the hybrid observer.

### Effect of realignment on the position estimation error

The same experiment of Fig. 9 has been repeated after a better realignment of the two motor shafts, operated by means of a laser alignment equipment. Fig. 11 shows a comparison of the position error (difference between the measured electrical position and the observed one) during the first seconds of the two tests, that is in the low speed region. A better alignment mitigates the position error and its harmonic content.

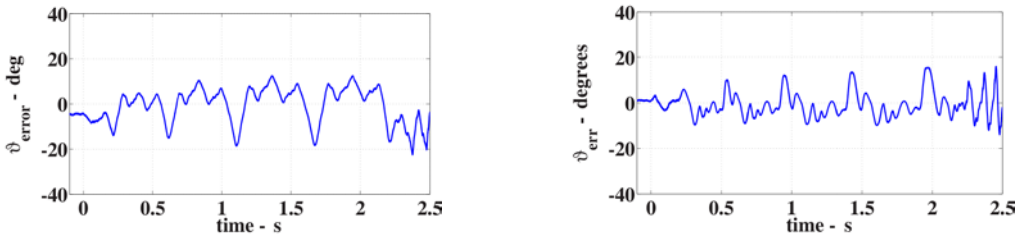


a) b)

Fig. 11: Detail of the position estimation error at low speed during the torque control test of Fig. 8. a) before the realignment (same as Fig. 8); b) after the laser realignment.

### Speed sensorless control

The sensorless speed control is last presented in Fig. 12. The motor is loaded at 60 Nm at time 0s (low speed, loaded condition). At time 2 s a speed ramp is applied up to 500 rpm (high speed, loaded condition). At time 7 s the load is removed (high speed, no load condition). The transition between the low speed and the high speed model in the hybrid sensorless observer is evidenced by the different nature of the noise superimposed to the position error and the $i_q$ current waveforms (second and fourth subplots in Fig. 12). The transition occurs around time 2.5 s.
The control showed to be robust in all the reported working conditions. Still the current high speed is noisy due to the back-EMF harmonics. Moreover, the position estimation at low speed is very sensitive to load conditions due to the very limited saliency of the machine.

## Conclusion

The sensorless control of an axial flux permanent magnet motor drive has been proposed and tested. The control is based on a simple hybrid flux observer scheme. The very weak saliency of the motor produces position estimation errors and sensitivity to mechanical misalignments at low speed, while the back-emf harmonics produce position noise and speed estimation ripple in the rest of the speed range. Still the control shows to be robust in all the speed range, at no load and load.

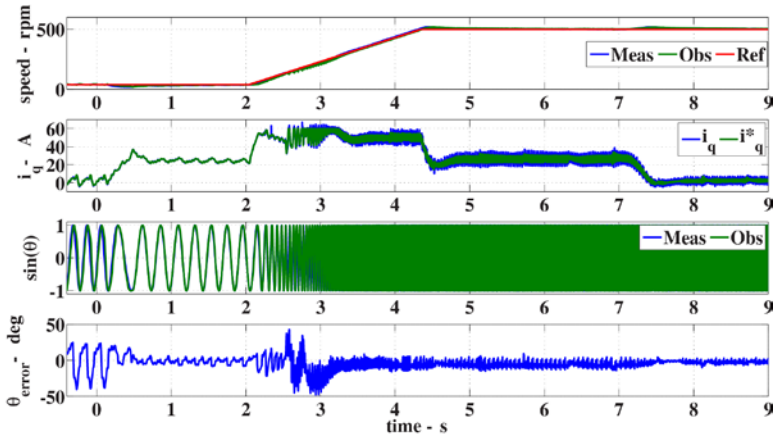


Fig. 12: Sensorless speed control in the range 40 rpm - 500 rpm, at load and no load.

# References


[1] J. Gieras, R. Wang, M. Kamper, “Axial Flux Permanent Magnet Brushless Machines,” (book), Springer Verlag, 2008, ISBN 1402069936

[2] Caricchi, F.; Crescimbini, F.; Mezzetti, F.; Santini, E.; "Multistage axial-flux PM machine for wheel direct drive," *Industry Applications, IEEE Transactions on* , vol.32, no.4, pp.882-888, Jul/Aug 1996

[3] Yicheng Chen; Pillay, P.; Khan, A.; "PM wind generator topologies," *Industry Applications, IEEE Transactions on* , vol.41, no.6, pp. 1619- 1626, Nov.-Dec. 2005

[4] Jansen, P.L.; Lorenz, R.D.; "Transducerless field orientation concepts employing saturation-induced saliencies in induction machines," *Industry Applications, IEEE Transactions on* , vol.32, no.6, pp.1380-1393, Nov/Dec 1996

[5] Linke, M.; Kennel, R.; Holtz, J.; , "Sensorless position control of permanent magnet synchronous machines without limitation at zero speed," *IECON 02 [Industrial Electronics Society, IEEE 2002 28th Annual Conference of the]* , vol.1, no., pp. 674- 679 vol.1, 5-8 Nov. 2002

[6] César Silva, G.M. Asher and M. Sumner, “Hybrid rotor position observer for wide speed-range sensorless PM motor drives including zero speed”, Proc. on IEEE Transactions on Industrial Electronics, Vol. 53, N.2, April 2006, pp. 373-378

[7] G.D. Andreescu, C.I. Pitic, F. Blaabjerg and I. Boldea, “Combined flux observer with signal injection enhancement for wide speed range sensorless direct torque control of IPMSM drives”, Proc. in IEEE Transactions on Energy Conversion, Vol. 23, N. 2, June 2008, pp. 393-402

[8] Wisniewski, J.; Koczara, W.; "Sensorless control of the axial flux permanent magnet synchronous motor at standstill and at low speed," *Compatibility and Power Electronics, 2009. CPE '09.* , vol., no., pp.463-468, 20-22 May 2009

[9] R.H. Moncada, J.A. Tapia and T.M. Jahns, “Analysis of negative-saliency permanent-magnet machines”, Proc. IEEE Transaction on Industrial Electronics, Vol. 57, N. 1, January 2010, pp. 122-127

[10] N. Bianchi, S. Bolognani, and B. J. Chalmers, “Salient-rotor PM synchronous motors for extended flux-weakening operation range”, IEEE Trans. Ind. Appl., vol. 36, no. 4, pp. 1118–1125, Jul./Aug. 2000

[11] http://www.hoganas.com/en/Products--Applications/Soft-Magnetic-Composites/

[12] Bojoi, R.; Guglielmi, P.; Pellegrino, G.-M.; "Sensorless Direct Field-Oriented Control of Three-Phase Induction Motor Drives for Low-Cost Applications," *Industry Applications, IEEE Transactions on* , vol.44, no.2, pp.475-481, March-april 2008

[13] Corley, M.J.; Lorenz, R.D.; "Rotor position and velocity estimation for a salient-pole permanent magnet synchronous machine at standstill and high speeds," *Industry Applications, IEEE Transactions on* , vol.34, no.4, pp.784-789, Jul/Aug 1998